Proposed mechanism for regulation of H_2O_2-induced programmed cell death in plants by binding of cytochrome *c* to 14-3-3 proteins

The cytochrome *c*/14-3-3 complex in plant programmed cell death

Carlos A. Elena-Real[1], Katiuska González-Arzola[1], Gonzalo Pérez-Mejías[1], Antonio Díaz-Quintana[1], Adrián Velázquez-Campoy[2-6], Bénédicte Desvoyes[7], Crisanto Gutiérrez[7], Miguel A. De la Rosa[1], Irene Díaz-Moreno[1]

[1]Instituto de Investigaciones Químicas (IIQ) – Centro de Investigaciones Científicas Isla de la Cartuja (cicCartuja), Universidad de Sevilla – Consejo Superior de Investigaciones Científicas (CSIC), Avda. Américo Vespucio 49, Sevilla 41092, Spain.

[2]Institute of Biocomputation and Physics of Complex Systems (BIFI), Joint Units IQFR-CSIC-BIFI, and GBsC-CSIC-BIFI, Universidad de Zaragoza, Zaragoza 50018, Spain.

[3]Department of Biochemistry and Molecular and Cell Biology, Universidad de Zaragoza, Zaragoza 50009, Spain.

[4]Aragon Institute for Health Research (IIS Aragon), Zaragoza, 50009, Spain

[5]Biomedical Research Networking Centre for Liver and Digestive Diseases (CIBERehd), Madrid 28029, Spain.

[6]Fundacion ARAID, Government of Aragon, Zaragoza 50018, Spain.

[7]Centro de Biología Molecular Severo Ochoa, CSIC-UAM, Nicolás Cabrera 1, Cantoblanco, 28049 Madrid, Spain.

Corresponding authors:

Miguel A. De la Rosa & Irene Díaz-Moreno, Instituto de Investigaciones Químicas (IIQ) – Centro de Investigaciones Científicas Isla de la Cartuja (cicCartuja), Universidad de Sevilla – Consejo Superior de Investigaciones Científicas (CSIC), Avda. Américo Vespucio 49, Sevilla 41092, Spain. Tel: +34 954489513;
E-mail: marosa@us.es; idiazmoreno@us.es

SUMMARY

Programmed cell death is crucial for development and homeostasis of all living organisms. In human cells, the double role of extra-mitochondrial cytochrome *c* in triggering apoptosis and inhibiting survival pathways is well reported. In plants, however, the specific role of cytochrome *c* upon release from the mitochondria remains in part veiled yet death stimuli do trigger cytochrome *c* translocation as well. Here, we identify an *Arabidopsis thaliana* 14-3-3ι isoform as a cytosolic cytochrome *c* target and inhibitor of caspase-like activity. This finding establishes the 14-3-3ι protein as a relevant factor at the onset of plant H_2O_2-induced programmed cell death. The *in vivo* and *in vitro* studies herein reported reveal that the interaction between cytochrome *c* and 14-3-3ι exhibits noticeable similarities with the complex formed by their human orthologues. Further analysis of the heterologous complexes between human and plant cytochrome *c* with plant 14-3-3ι and human 14-3-3ε isoforms corroborated common features. These results suggest that cytochrome *c* blocks p14-3-3ι so as to inhibit caspase-like proteases, which in turn promote cell death upon H_2O_2-treatment. Besides establishing common biochemical features between human and plant programmed cell death, this work sheds light onto the signaling networks of plant cell death.

SIGNIFICANT STATEMENT

Common features of the cytochrome *c*-dependent pathways leading to programmed cell death in plants and humans are herein revealed. In response to oxidative stress, cytochrome *c* is released from mitochondria to the cytoplasm to hamper the iota isoform of the 14-3-3 protein family, thereby decreasing inhibition of caspase-like activity and likely contributing to promote cell death in plants.

KEYWORDS

Cytochrome *c* / 14-3-3 protein family / NMR / ITC / Programmed Cell Death / Arabidopsis

INTRODUCTION

Programmed Cell Death (PCD) is an essential process for the development and homeostasis of the whole range of multicellular organisms. Different signaling mechanisms triggering PCD have been proposed in a diverse range of species. Still, evolutionarily distant organisms – including humans and plants – share common features during the onset of PCD (Daneva *et al*., 2016). Indeed, evolution has conserved the release of cytochrome *c* (C*c*) from the mitochondria into the cytoplasm, an event found in yeast, plants, flies and humans (Li *et al*., 1997; Balk *et al*., 1999; Arama *et al.,* 2006; Giannattasio *et al*., 2008). In humans, C*c* interacts with the apoptotic protease-activating factor-1 (Apaf-1) in the cytosol, initiating caspase-9 recruitment and formation of the apoptosome (Riedl *et al*., 2005). Apoptosome assembly, in turn, drives the activation of caspase-3 and -7, which execute cell death. In plants, however, the absence of an Apaf-1 homologue makes the role of cytosolic C*c* intriguing. In fact, despite plants contain caspase-like enzymes such as metacaspases (Fagundes *et al*., 2015), saspases (Coffeen *et al*., 2004) and phytaspases (Chichkova *et al*., 2010), whether C*c* can trigger or modulate their activities remains unknown.

The recent discovery of extra-mitochondrial C*c* targets in humans and plants under PCD conditions (Martínez-Fábregas *et al*., 2013; 2014a) suggests that C*c* mediates additional pathways in PCD beyond apoptosome formation. Besides, it has been described that post-translational modifications of C*c* exerts further modulation of mitochondrial and PCD-related functions (Rodríguez-Roldán *et al.*, 2008; García-Heredia *et al.*, 2011; Guerra-Castellano *et al.*, 2016; Moreno-Beltran *et al.*, 2017; Guerra-Castellano *et al.*, 2018; Kalpage *et al.*, 2020). Furthermore, we have recently demonstrated that C*c* inhibits the histone chaperone function of human SET/TAF-Iβ (González-Arzola *et al*., 2015) and its orthologue NRP1 in *Arabidopsis* (González-Arzola *et al*., 2017), probably affecting the DNA repair machinery during PCD (Díaz-Moreno *et al*., 2018). These findings support the existence of common C*c*-mediated routes that impair pro-survival pathways during PCD in humans and plants (Martínez-Fábregas *et al.*, 2014b).

In mammals, C*c* blocks 14-3-3ε – an Apaf-1 inhibitory protein – aiding caspase cascade activation during apoptosis (Kim *et al*., 2012; Elena-Real *et al*., 2018). 14-3-3 proteins constitute a highly evolutionarily conserved protein family in eukaryotes. Specifically, *Arabidopsis thaliana* expresses thirteen 14-3-3 isoforms (also referred to as GF14 proteins), which can be classified as epsilon (μ, ε, π, ι, ο) or non-epsilon (κ, λ, ψ, ν, υ, ω, ϕ, χ) isoforms (Jasper *et al*., 2011; Uversky *et al*., 2014). 14-3-3 proteins form homo-/heterodimers. The nine α-helices of each monomer form an amphipathic groove in the dimer to which Ser/Thr phosphorylated targets bind (Yang *et al*., 2006). 14-3-3 proteins also participate in phosphorylation-independent interactions (Petosa *et al*., 1998; Masters *et al*., 1999; Aachmann *et al*., 2007). Plant 14-3-3 proteins are involved in vital processes such as primary metabolism (Cotelle *et al*., 2000), stress tolerance (Yan *et al*., 2004) and plant development (van Kleeff *et al*., 2014). In addition, mitogen-activated kinases (MAPKs), which are critical for some types of PCD (Boualem *et al*., 2016), interact with 14-3-3 proteins (Lalle *et al.,* 2005). However, the specific role for 14-3-3 proteins in plant PCD remains veiled.

Based on animal data, it is tentative to think that 14-3-3 proteins could modulate caspase activity in plants. So we sought to discover whether C*c* could interact with any plant 14-3-3 protein, as does it with the human 14-3-3ε isoform (h14-3-3ε). Based on sequence similarity and electrostatic surface potential analysis, here we identify the plant 14-3-3ι isoform (p14-3-3ι) as the most related *Arabidopsis* 14-3-3 protein to h14-3-3ε. We also report that p14-3-3ι inhibits caspase-3-like activity, probably by acting as a negative regulator of H_2O_2-induced PCD, like its human orthologue h14-3-3ε. The interaction between p14-3-3ι and *Arabidopsis* C*c* (pC*c*) has been detected *in cell* and further characterized *in vitro* by using a couple of biophysical techniques, namely Isothermal Titration Calorimetry (ITC) and Nuclear Magnetic Resonance (NMR), so as to highlight its similarities with human cytochrome *c* (hC*c*) and h14-3-3ε. The formation of heterologous complexes between C*c* (from humans and plants) and both 14-3-3 orthologues have also been studied *in cell* and *in vitro*. Altogether, the similarities between the physiological and heterologous complexes suggest that the interactions involving C*c* and 14-3-3 proteins following PCD stimuli are evolutionarily conserved throughout eukaryotes.

RESULTS

14-3-3ι is the closest related protein to human 14-3-3ε and inhibits caspase-3-like activity in plant cells

The human 14-3-3ε protein (h14-3-3ε) is a versatile protein crucial in several processes, including PCD as it can bind and block both Apaf-1 and C*c* (Kim *et al*., 2012; Elena-Real *et al*., 2018). Although 14-3-3 proteins are evolutionarily conserved in eukaryotes, the function of these proteins in plant PCD is hardly understood. To elucidate the functions of *A. thaliana* 14-3-3 proteins, a search for proteins exhibiting high sequence similarity to h14-3-3ε in this organism was performed. Multiple sequence alignments of h14-3-3ε, p14-3-3ι and plant 14-3-3ε (p14-3-3ε) were carried out using the Clustal Omega program (Figure 1a) (Sievers *et al*., 2011). Notably, h14-3-3ε and p14-3-3ι displayed a 76% sequence identity and an 85% sequence homology. These values are slightly lower for the h14-3-3ε and p14-3-3ε pair (71% identity and 84% homology). The similarity between p14-3-3ι and p14-3-3ε sequences was also checked, showing a 73% and 86% identity and homology, respectively. A cladogram built from sequence alignments of thirteen plant 14-3-3 isoforms clearly demonstrated that p14-3-3ι is a closer orthologue to h14-3-3ε than p14-3-3ε (Figure 1b).

Also the surface electrostatic potential plays a key role in protein-protein interactions, in particular when positively-charged proteins as C*c* are involved. As there were no three-dimensional structures available for p14-3-3ι nor for p14-3-3ε, we constructed homology models based on X-ray diffraction data from h14-3-3ε homologues (PDB code, 2BR9). As can be seen in Figure 1c, the electrostatic surface potential distribution of h14-3-3ε and p14-3-3ι were similar at 100 mM ionic strength, however, that of p14-3-3ε shows prominent positively-charged regions. Altogether, the amino acid sequence analysis and the electrostatic surface properties indicate that p14-3-3ι is more closely related than p14-3-3ε to h14-3-3ε.

In humans, h14-3-3ε prevents apoptosis progression by interacting with some apoptotic factors, namely Bax (Nomura *et al.*, 2002) and Apaf-1 (Kim *et al.*, 2012),

impairing caspase cascade activation. In plants, a similar role for p14-3-3ι in PCD is still unknown. To unveil the possible effect of such plant 14-3-3 family members during the cellular response upon PCD, protoplasts from *A. thaliana* were transfected with an expression vector that encodes for p14-3-3ι. Cells that underwent PCD by 35 mM H_2O_2 treatment were collected at different times to monitor cell survival. Interestingly, p14-3-3ι-transfected protoplasts showed slightly higher cell viability than protoplasts transfected with the empty vector after 90 min treatment (Figure 2a, Table S1). This suggests a protective effect of p14-3-3ι in those cells undergoing PCD. Moreover, protoplasts transfected with pC*c* displayed a little lower cell viability than protoplasts transfected with the empty vector upon oxidative stress (Figure S1, Table S2).

To further explore whether the enhancement in cell viability correlates with a less efficiency in caspase-3-like activation, we measured such activity in MM2d *A. thaliana* cells. In fact, caspase-like activity has been previously detected during PCD (Fagundes *et al*., 2015), since there are no human caspase homologues in plants. Caspase-like activity was thus assessed by incubating a caspase-3 substrate tethered to the fluorophore 7-amino-4-methylcoumarin (AMC) with extracts from non-treated and H_2O_2-treated MM2d cells for 8 h (Figure 2b, Table S3). As can be seen in Figure S2a,b, caspase-3 like activity was maximum after 8 h H_2O_2 treatment, in agreement with previous reports from our group (García-Heredia *et al*., 2008). As expected, the caspase-3-like activity was notably higher in the extracts from H_2O_2-treated cells (Figure 2b), indicating H_2O_2 triggers PCD and, therefore, the activation of caspase-like proteases, as previously reported (García-Heredia *et al*., 2008). Extracts from H_2O_2-treated cells were titrated with increasing concentrations of p14-3-3ι, and caspase-3-like activity was measured (Figure 2b). Strikingly, increasing concentrations of p14-3-3ι resulted in a lower caspase-3-like activity. Indeed, addition of 10 μM p14-3-3ι caused caspase activity to drop to 60%. Notably, this finding is consistent with the role proposed for human analogues of p14-3-3ι (Kim *et al*., 2012) and suggests a putative role for this protein family in plants.

Extra-mitochondrial plant C*c* interacts with p14-3-3ι in MM2d cells

In light of the above results, we sought to better understand the mechanisms operating in such PCD-related protease inhibition. Hence, the focus of the study shifted to 14-3-3 family interacting proteins (i.e. C*c*). The interaction between hC*c* and h14-3-3ε has recently been demonstrated in human cells during PCD (Martinez-Fábregas *et al*., 2014; Elena-Real *et al*., 2018). Given the homology between h14-3-3ε and p14-3-3ι, we tested if p14-3-3ι could interact with pC*c* in cells undergoing H_2O_2-induced PCD. Accordingly, Bimolecular Fluorescence Complementation (BiFC) experiments were carried out in A. thaliana protoplasts under H_2O_2 treatment.

The release of pC*c* from mitochondria towards the cytoplasm of *A. thaliana* root cells under such oxidative stress conditions was corroborated by immunodetection of pC*c* in a plant line that expresses YFP in the mitochondria, 35S:Mt-YFP (mt-CD3-990) (Nelson el al., 2007; Vellosillo el al., 2013) (Figure 3a). A punctuated fluorescence pattern that colocalize with YFP was observed in the absence of peroxide treatment (Figure 3a and S3a), which is indicative of mitochondrial pC*c* localization, as reported for other plant mitochondrial proteins (Nagaoka *et al*., 2017). The fluorescence signal of pC*c* became diffuse upon H_2O_2 treatment and no longer colocalizes with the YFP mitochondrial marker (Figure 3a - right panel and S3b). Moreover, the localization of full-length pC*c* fusion protein with GFP (pC*c*-GFP) was analyzed in transfected protoplasts (Figure 3b). In homeostasis, pC*c*-GFP showed a mitochondrial localization, whereas pC*c*-GFP leaves the mitochondria and spreads into the cytoplasm upon H_2O_2 treatment of *A. thaliana* protoplast cells. Altogether, these data support that pC*c* leaves mitochondria under PCD signaling.

Then, BiFC assays were performed to test whether pC*c* and p14-3-3ι recognize each other *in cell*. cDNAs encoding p14-3-3ι and pC*c* were fused to the N-terminal and C-terminal fragments of the yellow fluorescent protein (YFP), respectively. The resulting vectors were co-delivered into *A. thaliana* protoplasts, and fluorescence was detected after YFP reconstitution. As shown in Figure 3c, YFP reconstitution was observed in the cytoplasm, only when pC*c* and p14-3-3ι cDNAs were used to transfect *Arabidopsis* protoplasts and were H_2O_2-treated, indicating an interaction between both proteins only after oxidative stress. Actually, previous results from our group demonstrated that YFP reconstitution in

BIFC assays did not occur since C*c*-CYFP remained in the mitochondria while p14-3-3ι-NYFP was in the cytoplasm (Martínez-Fábregas *et al.*, 2013). Overlay of YFP reconstitution with MitoTracker and chlorophyll autofluorescence suggests that interaction between pC*c* and p14-3-3ι under H_2O_2-induced PCD occurs mainly in the cytosol (Figure 3c).

p14-3-3ι forms a well-defined complex with pC*c*

To assess the affinity between pC*c* and p14-3-3ι, isothermal titration calorimetry (ITC) experiments were carried out. Analysis of the ITC thermogram showed pC*c* bound p14-3-3ι with a stoichiometry of 1.9, indicating two molecules of pC*c* bind a p14-3-3ι dimer (Figures 4a, S4a, upper panel). The dissociation constant (K_D) for the interaction is 8.5 μM, which is similar to the value recently reported for the hC*c* / h14-3-3ε complex (Elena-Real *et al*., 2018).

1D ^{1}H NMR spectra were also recorded and the ε-methyl signal of Met88 – the residue providing the 6th ligand of the heme group – was followed upon titration of pC*c* with p14-3-3ι. The resonance signal of reduced pC*c* (Fe^{2+}) broadened at increasing concentrations of p14-3-3ι, suggesting complex formation (Figure S4a, middle panel). To unveil pC*c* residues involved in the recognition of p14-3-3ι, 2D [^{1}H, ^{15}N] HSQC spectra of ^{15}N-labeled pC*c* were recorded. Titration of p14-3-3ι caused an overall broadening of pC*c* amide signals, also due to complex formation (Figure S4a, lower panel). In addition, several pC*c* amide signals specifically underwent larger changes in ^{1}H line widths (^{1}H $\Delta\Delta\nu_{1/2\ Binding}$) upon p14-3-3ι binding, indicating that the corresponding residues were located at, or near the complex interface. Moreover, chemical-shift perturbations (CSPs) were observed in a small number of amide signals upon p14-3-3ι addition. Altogether, line broadening and CSPs of the pC*c* signals detected upon the addition of p14-3-3ι were mapped onto the surface of pC*c* (Figure 4a). The resulting map reveals that pC*c* recognizes p14-3-3ι mainly using the surface surrounding the heme cleft, as described for the human hC*c* / 14-3-3ε complex (Elena-Real *et al*., 2018). This finding also agrees with the surface area used by C*c* and functionally related proteins when interacting with its redox partners in the electron transport chain

(Medina *et al.*, 1992; Navarro *et al.*, 1995a; 1995b; De la Cerda *et al.*, 1997; Sun *et al.*, 1999; Frazão *et al.*, 2001; Goñi *et al.*, 2009; Hervás *et al*., 2013; Moreno-Beltrán *et al*., 2014, 2015, 2017). In addition, the behavior of the NMR signals indicates an intermediate exchange rate on the NMR scale, in accordance with the K_D value within the μM range inferred from ITC assays.

Previous studies have described that the C-terminal tails of h14-3-3ε are involved in the interaction with hC*c* (Elena-Real *et al*., 2018). To check whether the C-terminal tails of p14-3-3ι (p14-3-3ι$_{240-268}$) also participate in the recognition of pC*c*, the metalloprotein was titrated with the p14-3-3ι$_{240-268}$ peptide, and the NMR signals in 2D [^{1}H, ^{15}N] HSQC spectra were monitored. Interestingly, no substantial CSPs or line broadening were observed on ^{15}N-labeled pC*c* amide signals upon p14-3-3ι$_{240-268}$ addition (Figure S5a,b, left panels), suggesting the C-terminal tails of p14-3-3ι are not involved in the interaction with pC*c*. The inability of p14-3-3ι$_{240-268}$ to interact with pC*c* was also corroborated by ITC experiments (Figure S5c, left panel).

Despite small differences between p14-3-3ι and p14-3-3ε, the C-terminal tails of p14-3-3ε have a length nearer to those of h14-3-3ε (Figure 1a). Thus, we checked whether p14-3-3ε C-terminal tails (p14-3-3ε$_{235-254}$) interacted with pC*c*. To that end, ^{15}N-labeled pC*c* was titrated with p14-3-3ε$_{235-254}$, and the behavior of NMR amide signals was followed again by 2D [^{1}H, ^{15}N] HSQC spectra. As in the titration with p14-3-3ι$_{240-268}$, pC*c* amide signals did not experience substantial CSPs or line broadening (Figure S5a,b, right panels), indicating neither C-terminal tails of the epsilon or iota 14-3-3 isoforms interact with pC*c*. To confirm this result, an ITC experiment was performed titrating pC*c* with p14-3-3ε$_{235-254}$. The thermogram corroborated the absence of any interaction between pC*c* and the p14-3-3ε C-terminal tails (Figure S5c, right panel).

Human and plant C*c* complexes with 14-3-3 proteins display similar conformations

To further explore the interaction between C*c* and 14-3-3 proteins in both humans and plants, we studied the heterologous complexes of both hC*c* and pC*c* with

h14-3-3ι and p14-3-3ε. Accordingly, interactions were assessed in HEK293T human cells by BiFC analysis. Cells were transfected with C*c* and 14-3-3 proteins cloned into mammalian vectors cYFP and nYFP, respectively. PCD was triggered by treating cells with 10 μM CPT for 6 h. YFP reconstitution showed the plant complex pC*c* / p14-3-3ι could be assembled in human cells, whilst YFP was also reconstituted when heterologous complexes (hC*c* / p14-3-3ι and pC*c* / h14-3-3ε) were analyzed (Figure S6). These data suggest a great similarity between both physiologic and cross-complexes, hinting that interactions between C*c* and 14-3-3 proteins are conserved across evolution.

As the BiFC analysis demonstrated both heterologous complexes can be assembled, ITC and NMR titrations were performed to corroborate these interactions. Thermograms for both hC*c* / p14-3-3ι and pC*c* / h14-3-3ε complexes exhibited a stoichiometry of 1.6 – suggesting that two molecules of C*c* recognize the 14-3-3 dimer – as well as similar enthalpy values and K_D values in the μM range (Figure 4b,c). These data agree with those evidenced for the pC*c* / p14-3-3ι complex, although the K_D value of pC*c* interacting with h14-3-3ε is slightly higher (29 μM).

As in the plant physiological complex, the ε-methyl ^{1}H NMR signal of both hC*c* and pC*c* axial ligands of the heme group (Met80 and Met88, respectively) broadened during the titration with 14-3-3 proteins – due to cross-complex formation (Figure S4b,c). Likewise, backbone amide signals of both C*c* species underwent specific broadening in 2D [^{1}H, ^{15}N] HSQC spectra. The resulting maps of the perturbed resonances evidenced that both C*c* species use similar surfaces to recognize their 14-3-3 targets from both human and plants (Figure 4b,c).

Given hC*c* interacts with the C-terminal tails of its human 14-3-3 target (Elena-Real *et al*., 2018), we investigated whether it could also recognize the C-terminal tails of p14-3-3ι (p14-3-3ι$_{240-268}$). To achieve this, an ITC titration was carried out producing a K_D value of 24.9 μM, which confirmed such recognition (Figure 5a). In addition, ^{15}N-labeled hC*c* was titrated with increasing concentrations of p14-3-3ι$_{240-268}$, and the interaction was followed by recording [^{1}H, ^{15}N] HSQC spectra (Figure 5b). Significant CSPs of hC*c* resonances were observed upon p14-3-3ι$_{240-268}$ titration (Figure 5c) highlighting complex formation. These shifts were

mapped onto the surface of C*c*, revealing the regions involved in the recognition of p14-3-3ι$_{240\text{-}268}$ (Figure 5d).

DISCUSSION

Despite the obvious differences found in human and plant PCD – owing to distinct cellular and physiological organization – essential molecular events have been evolutionarily conserved. The release of C*c* from the mitochondria to the cytosol upon death stimuli is one of such preserved events. This translocation makes sense after the recent discovery of new cytosolic and nuclear C*c*-targets, which are common to humans and plants, and can thus be considered functional analogues (Martínez-Fábregas *et al*., 2013; 2014a; 2014b). Indeed, the similar roles fulfilled by the common targets, as well as the C*c*-mediated inhibition of their functions, support evolutionarily conserved PCD regulating mechanisms (Díaz-Moreno *et al*., 2018; González-Arzola *et al*., 2015; 2017). Furthermore, among these targets, h14-3-3ε stands out due to its inhibitory role in human PCD, which is impaired through its interaction with hC*c*. In plants, the presence of several 14-3-3 protein isoforms which share sequence and structural features with the human 14-3-3 protein family hinted at their function also being preserved. C*c* blocks p14-3-3ι to inhibit caspase-like proteases, which in turn are thought to promote cell death upon H_2O_2-treatment (Figure 6). The precise mechanism underlying such inhibition remains unclear, although it is well known that 14-3-3 proteins interact with certain plant protein kinases which are active upon PCD, such as MAP kinases (Muslin *et al*., 1996; Lalle *et al*., 2005). Specifically, MAP kinases act as signaling factors in some forms of PCD – as in the hypersensitive response – in which caspase-like proteases become active. Thus, a mechanism by which 14-3-3 proteins could inhibit caspase-like activities through the modulation of MAP kinases can be foreseen, but further work is needed to shed further light on such an intricate pathway responsible for cell fate decisions.

We have also confirmed that pC*c* is released from mitochondria under PCD conditions and we demonstrated the interaction between such hemeprotein and p14-3-3ι – suggesting that both proteins take part in death signaling in plants. Certainly, the moderate affinity of the pC*c* / p14-3-3ι interaction revealed by ITC is similar to those exhibited by their human counterparts. This is consistent with

a transient interaction that may allow pC*c* to modulate the p14-3-3ι functionality after the massive release of C*c* from the mitochondria into the cytosol, as occurs in humans.

The biochemical similarities found between the C*c* / 14-3-3 protein complexes from humans and plants are highlighted under the comparative analysis of physiological and heterologous complexes. For instance, in all complexes, C*c* species use the same surface region to interact with 14-3-3 proteins. This interface involves residues surrounding the heme cleft – which are also used to recognize C*c* redox partners (Hervás *et al*., 2013; Moreno-Beltrán *et al*., 2014; 2015; 2017). In addition, the K_D values of these complexes are in the same range, although small differences in affinity are exhibited, especially that of the heterologous complex pC*c* / 14-3-3ε. In addition, amide resonances of pC*c* broaden less than those from hC*c* in complex with 14-3-3 proteins. Such behavior can be explained because hC*c* also recognizes the C-terminal tails of 14-3-3 proteins. Then, the C-terminal tails modulate in somehow the lifetime of both physiological and heterologous hC*c*-involving complexes, although further analysis to determine the association and dissociation rates of such interactions will be needed.

Overall, the C*c* / 14-3-3 protein complexes have evolved to conserve the same main features which allows them to carry out similar functions. Slight differences in the recognition mode have been acquired; to subtly adapt the biochemical pathways to the distinct cellular organization found in humans and plants. Such differences, however, do not prevent both organisms from using similar routes to trigger PCD, by utilizing conserved proteins.

EXPERIMENTAL PROCEDURES

Human cell cultures

HeLa and Human Embrionic Kidney 293T (HEK293T) cells were cultured in Dulbecco's modified Eagle's medium (DMEM), supplemented with 10% heat-inactivated fetal bovine serum (FBS), 2 mM L-glutamine, 100 U/mL penicillin and

100 μg/mL streptomycin. Cell cultures were maintained at 37 ºC in a humidified 5% CO_2 atmosphere.

Arabidopsis thaliana MMd2 cells

A. thaliana MM2d cells (Menges and Murray, 2002) were grown in 1 x Murashige and Skoog (MS) medium (Duchefa Biochemie), supplemented with 30 g/L sucrose (Sigma-Aldrich), 0.5 mg/L NAA (Sigma-Aldrich), 0.05 mg/L kinetin (Sigma-Aldrich), 200 mg/L cefotaxime (Duchefa Biochemie) and 200 mg/L penicillin (Duchefa Biochemie). Cell cultures were maintained in a shaking incubator at 100 rpm and 25 °C.

For caspase-3-like assays, *A. thaliana* MMd2 cells were treated with 35 mM H_2O_2 for 8 h. Treated and non-treated cell cultures were centrifuged at 3,000 x g for 3 min, and pelleted cells were suspended in 20 mM Hepes-KOH buffer (pH 7.5), supplemented with 10 mM KCl, 1.5 mM $MgCl_2$, 1 mM EDTA, 1 mM EGTA, 1 mM DTT and 0.1 mM PMSF. Cell suspensions were lysed by 30 s sonication and centrifuged at 12,000 x g for 15 min. After discarding the pellets, the supernatants were used as cell extracts for enzymatic assays.

A. thaliana protoplast viability assays

Protoplasts from MM2d cells were obtained incubating them with MS-Glucose/Mannitol (0.34 M) buffer, supplemented with 1% cellulase and 0.2% macerozyme, during 3 h at 25 ºC. Then, cells were washed twice with MS-Glucose/Mannitol (0.34 M) buffer, and once with MS-Sucrose (0.28 M) buffer. Protoplasts were obtained from the supernatant.

Protoplast transfection was carried out by following the protocol described by Yoo *et al.* (2007). Briefly, 2 x 10^4 protoplasts were incubated with 30 μg of either pSPYNE-p14-3-3ι or empty pSPYNE vector in the presence of 40% poly(ethylene glycol)-4000 and 100 mM $CaCl_2$ for 15 min. After incubation, protoplasts were washed with 2 mM MES-KOH (pH 5.7), 154 mM NaCl, 125 mM $CaCl_2$, 5 mM KCl.

12 h after transfection, PCD was induced by adding 35 mM H_2O_2 for 90 min. Viable cells were stained with 0.01% fluorescein diacetate (FDA), whereas non-viable cells were stained with 400 mg/L Evans blue. Cells were visualized on a Leica DM 6000B Microscope.

Caspase-3-like assays

Caspase-3-like activity was measured as previously described (Clarke *et al*., 2000) with small modifications. Recombinant 14-3-3ι was mixed with 50 μg of MM2d cell extract in 25 mM HEPES buffer (pH 5), supplemented with 10% sucrose, 0.1% 3-[(3-Cholamidopropyl)dimethylammonio]-1-propanesulfonate hydrate (CHAPS), 1 mM (Ethylenedinitrilo)tetraacetic acid (EDTA), 1 mM Dithiothreitol (DTT) and 75 μM acetyl-DEVD-7-amino-4-methylcoumarin (Ac-DEVD-AMD, Enzo Life Sciences), a fluorescent substrate specific for caspase-3/7. The mix was incubated at 30 ºC for 18 h. Reactions were stopped with 175 mM acetic acid, 1% sodium acetate. The increase in fluorescence resulting from Ac-DEVD-AMC cleavage was determined in a Cary Eclipse (Varian) fluorescence spectrophotometer, using an excitation wavelength of 360 nm and an emission wavelength of 460 nm. Each experimental data was the average of at least three independent measurements.

Immunodetection of pC*c* in *A. thaliana* root cells

Arabidopsis plants carrying a construct driving the expression of YFP in the mitochondria (mt-CD3-990) was used (Nelson *et al.,* 2007). Four-day-old plants were treated or not treated with 35 mM H_2O_2 for 4h. Plants were fixed in microtubule stabilizing buffer (MTSB) composed of 50 mM 1,4-piperazinediethanesulfonic acid (PIPES) (pH 6.9), 5 mM EGTA, 5 mM MgSO4, and 4% paraformaldehyde. Partial digestion of cell wall was performed by using 20 mg/mL driselase from *Basidiomycetes sp* (Sigma) during 45 min at 37 ºC. Cells were permeabilized with MTSB containing 10% DMSO and 3% NP-40. Immunodetection was performed with polyclonal anti-pC*c* (1:250 dilution) obtained by immunizing male rabbits with recombinant pC*c* and anti-GFP

(Ab5450 1:2000, Abcam) overnight at 4ºC, followed by 1 h incubation with secondary antibody (anti-Goat Alexa 555 and anti-Rabbit Alexa 488, 1:500, ThermoFisher). Nuclei were stained with DAPI. Images were obtained with a confocal laser scanning microscope (LSM800 - Zeiss). For co-localization analysis and estimation of pC*c* amount in mitochondria upon oxidative treatment, the values for mean intensity signal of pC*c* and YFP were measured using FIJI (Rueden *et al*., 2017).

Bimolecular fluorescence complementation assays in *A. thaliana* protoplasts

Protoplasts were generated from healthy 4-week-old *A. thaliana* leaves. Cell walls were removed by incubating leaves with an enzymatic solution (20 mM MES-KOH at pH 5.7, 400 mM mannitol, 10 mM $CaCl_2$, 20 mM KCl, 1% Celullose R-10, 0.25% Macerozyme R-10, 0.1% Bovine Serum Albumin) for 1 h at 25 ºC. The resulting solution was centrifuged at 100 x g for 3 min at 4 ºC and cells were washed twice with 2 mM MES-KOH (pH 5.7), 154 mM NaCl, 125 mM $CaCl_2$, 5 mM KCl. The final pellet was resuspended in 4 mM MES-KOH (pH 5.7), 0.4 M mannitol, 15 mM $MgCl_2$.

For transfection, a pSPYCE vector containing cDNA coding for plant cytochrome *c* (pC*c*; gen CYTC-2 (AT4G10040), as previously reported by Rodríguez-Roldán *et al.,* 2006) fused with the C-end fragment of YFP was used, along with a pSPYNE plasmid containing cDNA coding for plant 14-3-3ι (p14-3-3ι) bound to the N-end of the YFP (Walter *et al.,* 2004; Martínez-Fábregas *et al.,* 2013). Moreover, cDNA coding for pC*c* was cloned in the p35S-sfGFP plasmid, which was a generous gift by Yutaka Kodama (Addgene plasmid #80127, Fujii & Kodama, 2015).

In order to transfect protoplasts, 2 x 10^4 protoplasts were incubated with 30 μg of pSPYCE/pSPYNE Bimolecular Fluorescence Complementation (BiFC) vectors or p35S-sfGFP/p35S-sfGFP-pC*c* vector in the presence of 40% Poly(ethylene glycol)-4000 for 15 min. After incubation, protoplasts were washed with W5 solution (2 mM MES-KOH (pH 5.7), 154 mM NaCl, 125 mM $CaCl_2$, 5 mM KCl). PCD was induced by adding 35 mM H_2O_2 for 4 h. Protoplasts were incubated in

W5 solution with 100 nM MitoTracker CMX-ROS for 10 min at room temperature. Finally, the YFP reconstitution was monitored on a Leica DM 6000B Microscope.

Bimolecular fluorescence complementation assays in human HEK293T cells

HEK293T cells were grown in 24-well plates, containing 20 mm coverslips, with 500 μL of DMEM (in the absence of antibiotics) until a confluence of 70-80% was reached.

For transfection, a BiFC vector containing cDNA coding for pC*c* or hC*c* fused with the C-end fragment of YFP was used, along with a BiFC plasmid containing cDNA for p14-3-3ι or human 14-3-3ε (h14-3-3ε) bound to the N-end part of YFP (Gandía *et al.,* 2008; Martínez-Fábregas *et al.,* 2013). pBiFC-bJunYN155 and pBiFC-bFosYC155 were used as positive controls, whereas pBiFC-bJunYN155 and pBiFC-bFos ZipYC155 were employed as negative controls.

Cells were transfected with those constructs using the Lipofectamine 2000 Transfection Reagent (Invitrogen), following manufacturer recommendations. Then, transfected cells were incubated for 24 h at 37 ºC. PCD was induced with 10 μM camptothecin (CPT) for 6 h. *In vivo* binding was assessed through YFP reconstitution visualized with fluorescence microscopy on a Leica DM 6000B Microscope. Nuclei were stained with 4',6-diamidino-2-phenylindole (DAPI).

Cloning, expression and purification of recombinant proteins

hC*c* and pC*c* were expressed as previously described (Moreno-Beltrán *et al*. 2014, 2015; Guerra-Castellano *et al.*, 2015) in *E. coli* BL21 (DE3) cells. 25 mL of Luria-Bertani (LB) medium, supplemented with 100 μg/mL ampicillin pre-cultures were grown overnight at 37 ºC under shaking. 2.5 mL of the pre-culture was used to inoculate 2.5 L of LB medium. hC*c*- and pC*c*-yielding cell cultures were incubated at 30 ºC and 37 ºC, respectively, under 24 h shaking. Cells were centrifuged at 6,000 rpm for 10 min in an Avanti J-25 centrifuge (Beckman Coulter), resuspended in 1.5 mM borate buffer (pH 8.5) and sonicated for 4 min.

Cellular debris was eliminated by centrifugation (20,000 rpm, 30 min). For NMR measurements, ^{15}N-labeled hC*c* and pC*c* were produced in minimal media with $^{15}NH_4Cl$ as a unique nitrogen source. Both C*c* purifications were carried out by ionic chromatography in a carboxy-methylcellulose matrix. Fractions containing C*c* were concentrated in an Amicon cell, with a 3 KDa cut-off membrane, until the desired concentration was reached. Protein samples were dialyzed against 10 mM sodium phosphate (pH 7.4) or 5 mM sodium phosphate (pH 6.3) for ITC and NMR experiments, respectively.

p14-3-3ι was cloned into the pET28a vector under the T7 promotor using *Nde*I – *Not*I restriction sites and containing a N-terminal hexahistidine tag. Primers were 5'-AGCCATATGATGTCATCATCAGGATCC-3' and 5'-AGTGCGGCCGCTCA-CTCAGTGGCATCG-3'.

Expression of p14-3-3ι and h14-3-3ε was performed in *E. coli* BL21 (DE3) cells cultured in LB medium at 37 ºC. When an optical density at 600 nm of 0.6-0.8 was reached, protein expression was induced by adding 1 mM isopropyl-β-D-1-thiogalactopyranoside (IPTG). After 24 h at 30 ºC, the cells were harvested by centrifugation and resuspended in 20 mM Tris-HCl (pH 8), 800 mM NaCl, 10 mM imidazole. Cells were broken by sonication and insoluble debris was removed by centrifugation, as above. p14-3-3ι and h14-3-3ε were purified by affinity chromatography using a Ni Sepharose 6 Fast Flow column (GE Healthcare) and a 10-300 mM imidazole gradient for elution. Protein fractions were concentrated in an Amicon cell, with a 3 kDa cut-off membrane, up to reach the desired protein concentration and dialyzed against 10 mM sodium phosphate (pH 7.4) or 5 mM sodium phosphate (pH 6.3) for ITC and NMR experiments, respectively.

p14-3-3ι and p14-3-3ε C-terminal peptides (p14-3-3ι$_{240-268}$ and p14-3-3ε$_{235-254}$) were purchased from Genosphere Biotechnologies (France).

ITC measurements

Reduced pC*c* or hC*c* were titrated into p14-3-3ι or h14-3-3ε samples using Auto-ITC200 (Malvern Instruments, UK) at 25 ºC. The experiments consisted of 2-μL injections of 300 μM C*c* solution in 10 mM sodium phosphate buffer (pH 7.4) into

the sample cell, initially containing 20 μM p14-3-3ι or h14-3-3ε solution in the same buffer.

The p14-3-3$\iota_{240-268}$ and p14-3-3$\varepsilon_{235-254}$ peptides were titrated with reduced pC*c* in a Nano ITC Low Volume (TA Instruments, USA) at 25 ºC. The experiments consisted of 2-μL injections of 1 mM p14-3-3$\iota_{240-268}$ or p14-3-3$\varepsilon_{235-254}$ solution in 10 mM sodium phosphate buffer (pH 7.4) into the sample cell, initially containing 100 μM pC*c* solution in the same buffer.

In all experiments the reference cell was filled with distilled water. All solutions were degassed before titration. Titrant was injected at appropriate time intervals to ensure the thermal power signal returned to the base line prior to the next injection. To achieve homogeneous mixing in the cell, the stirring speed was maintained constant at 1,000 rpm in the Auto-ITC200, and 300 rpm in the Nano ITC Low Volume. The data, specifically the heat per injection normalized per mole of injectant vs. molar ratio, were analyzed with Origin 7.0 (OriginLab Corp.). Calibration and performance tests of the calorimeter were carried out conducting $CaCl_2$-EDTA titrations with solutions provided by the manufacturer.

NMR measurements

NMR titrations of reduced pC*c* with p14-3-3ι or h14-3-3ε, as well as of reduced hC*c* with p14-3-3ι were followed by recording 1D ^{1}H and 2D [^{1}H,^{15}N] HSQC spectra on a Bruker Avance 700 MHz spectrometer at 25 ºC. Samples containing 50 μM reduced ^{15}N-labelled pC*c* or hC*c* in 5 mM sodium phosphate buffer (pH 6.3) were titrated with unlabelled p14-3-3ι or h14-3-3ε solutions in the same buffer. 0.1 M sodium ascorbate and 10% D_2O were added to ensure the redox state and to adjust the lock signal, respectively. Water signal was suppressed according to the WATERGATE solvent suppression method (Piotto *et al.,* 1992). The interaction of reduced pC*c* or hC*c* with p14-3-3$\iota_{240-268}$ or p14-3-3$\varepsilon_{235-254}$ was performed on a Bruker Avance 600 MHz spectrometer, as previously described. Data were processed using TopSpin NMR 2.0 software (Bruker), and line broadening and chemical-shift perturbation analyses was performed with Sparky 3 NMR Assignment Program (T.D. Goddard and D.G. Kneller, University of

California – San Francisco, US). Chemical-shift perturbation binding curves were fitted using a 1:1 binding model.

Statistical analysis

Statistical analysis was performed using GraphPad Prism 7 Software and experimental data of at least three independent measurements. Statistical significance was estimated using Student´s t-test. A *p* value of < 0.05 was considered significant.

ACKNOWLEDGMENTS

The authors thank the NMR Facility at CITIUS (University of Seville), the Biointeractomics Platform at the cicCartuja (University of Seville-CSIC) and TA instruments.

This work was supported by the Spanish Ministry of Economy and Competitiveness (BFU2015-71017/BMC MINECO/FEDER, PGC2018-096049-B-I00 BIO/BMC MICINN/FEDER and RTI2018-094793-B-I00 MICIU), the Andalusian Government (BIO198, US-1254317, US-1257019, P18-FR-3487 and P18-HO-4091) and the Ramón Areces Foundation. CAER was recipient of a PhD fellowship from the Fundación Cámara – University of Seville. GPM was awarded a PhD fellowship from the Spanish Ministry of Education, Culture and Sport (FPU17/04604). The CBMSO receives institutional grants from Fundacion Ramon Areces and Banco de Santander.

AUTHORS CONTRIBUTION

CAER, ADQ, KGA, IDM and MAR designed the research; CAER cloned, expressed and purified recombinant proteins; CAER, KGA, GPM, BD and CG carried out cellular experiments; CAER and AVC performed and analysed ITC measurements; CAER, ADQ, and IDM performed and analysed NMR data; CAER, KGA, ADQ, IDM and MAR wrote the paper.

CONFLICT OF INTEREST

The authors declare no conflicts of interest.

SUPPORTING INFORMATION

Additional Supporting Information may be found in the online version of this article.

Figure S1. Effect of pC*c* on cell viability of *A. thaliana* cells.

Figure S2. Time-course of caspase-3-like activity in *Arabidopsis thaliana* cell extracts along treatment with 35 mM H_2O_2.

Figure S3. Co-localization analysis and estimation of pC*c* amount in *Arabidopsis thaliana* cells upon oxidative treatment.

Figure S4. ITC and NMR titrations of pC*c* with p14-3-3ι (a), hC*c* with p14-3-3ι (b) and pC*c* with h14-3-3ε (c).

Figure S5. NMR and ITC titrations of pC*c* with p14-3-3$\iota_{240\text{-}268}$ and p14-3-3$\varepsilon_{235\text{-}254}$ peptides**.**

Figure S6. *In cell* interactions of plant and human C*c* with plant and human 14-3-3 protein family members**.**

Table S1. Datasets corresponding to individual data points of Figure 2a (viability of *A. thaliana* MM2d protoplasts transfected with p14-3-3ι or empty vectors upon oxidative stress).

Table S2. Datasets corresponding to individual data points of Figure S1 (viability of *A. thaliana* MM2d protoplasts transfected with pC*c* or empty vectors upon oxidative stress).

Table S3. Datasets corresponding to individual data points of Figure 2b (relative caspase-3-like activity in non-treated and H_2O_2-treated MM2d cell extracts, upon adding p14-3-3 ι at varying concentration).

REFERENCES

Aachmann, F.L., Fomenko, D.E., Soragni, A., Gladyshev, V.N. and Dikiy, A. (2007) Solution structure of selenoprotein W and NMR analysis of its interaction with 14-3-3 Proteins. *J. Biol. Chem.* **282**, 37036-37044.

Altschul, S.F., Madden, T.L., Schäffer, A.A., Zhang, J., Zhang, Z., Miller, W. and Lipman, D.J. (1997) Gapped BLAST and PSI-BLAST: a new generation of protein database search programs. *Nucleic Acids Res*. **25**, 3389-3402.

Arama, E., Bader, M., Srivastava, M., Bergmann, A. and Steller, H. (2006) The two Drosophila cytochrome *c* proteins can function in both respiration and caspase activation*. EMBO. J.* **25**, 232-243.

Baker, N.A., Sept, D., Joseph, S., Holst, M.J. and McCammon, J.A. (2001) Electrostatics of nanosystems: application to microtubules and the ribosome. *Proc. Natl. Acad. Sci. USA*, **98**, 10037-10041.

Balk, J., Leaver, C.J. and McCabe, P.F. (1999) Translocation of cytochrome *c* from the mitochondria to the cytosol occurs during heat-induced programmed cell death in cucumber plants. *FEBS Lett*. **463**, 151-154.

Boualem, A., Dogimont, C. and Bendahmane, A. (2016) The battle for survival between viruses and their host plants. *Curr. Opin. Virol.* **17**, 32-38.

Clarke, A., Desikan, R., Hurst, R.D., Hancock, J.T. and Neill, S.J. (2000) NO way back: nitric oxide and programmed cell death in Arabidopsis thaliana suspension cultures. *Plant. J.* **24**, 667-677.

Coffeen, W.C. and Wolpert, T.J. (2004) Purification and characterization of serine proteases that exhibit caspase-like activity and are associated with programmed cell death in *Avena sativa. Plant Cell,* **16**, 857-873.

Cotelle, V., Meek, S.E.M., Provan, F., Milne, F.C., Morrice, N. and MacKintosh, C. (2000) 14-3-3s regulate global cleavage of their diverse binding partners in sugar-starved Arabidopsis cells. *EMBO J.* **19**, 2869-2876.

Chichkova, N.V., Shaw, J., Galiullina, R.A., Drury, G.E., Tuzhikov, A.I., Kim, S.H., Kalkum, M., Hong, T.B., Gorshkova, E.N., Torrance, L., Vartapetian, A.B. and Taliansky, M. (2010) Phytaspase, a relocalisable cell death promoting plant protease with caspase specificity. *EMBO J.* **29**, 1149-1161.

Daneva, A., Gao, Z., Durme, M.V. and Nowack, M.K. (2016) Functions and regulation of programmed cell death in plant development. *Annu. Rev. Cell. Dev. Biol.* **32**, 441-468.

Danon, A. (2014) Protoplast Preparation and Determination of Cell Death. *Bio-protocol,* **4**, e1149.

De la Cerda, B., Navarro, J. A., Hervás, M., and De la Rosa, M. A. (1997). Changes in the reaction mechanism of electron transfer from plastocyanin to photosystem I in the cyanobacterium *Synechocystis sp.* PCC 6803 as induced by site-directed mutagenesis of the copper protein. *Biochemistry*, **36**, 10125–10130.

Desper, R. and Gascuel, O. (2004) Theoretical foundation of the balanced minimum evolution method of phylogenetic inference and its relationship to weighted least-squares tree fitting. *Mol. Biol. Evol.* **21**, 587-598.

Díaz-Moreno, I., Velázquez-Cruz, A., Curran-French, S., Díaz-Quintana, A. and De la Rosa, M.A. (2018) Nuclear cytochrome *c* – a mitochondrial visitor regulating damage chromatin dynamics. *FEBS Lett.* **592**, 172-178.

Elena-Real, C.A., Díaz-Quintana, A., González-Arzola, K., Velázquez-Campoy, A., Orzaez, M., López-Rivas, A., Gil-Caballero, S., De la Rosa, M.A. and Díaz-Moreno I (2018) Cytochrome *c* speeds up caspase cascade activation by blocking 14-3-3ε-dependent Apaf-1 inhibition. *Cell. Death Dis.* **9**, 365.

Fagundes, D., Bohn, B., Cabreira, C., Leipelt, F., Dias, N., Bodanese-Zanettini, M.H. and Cagliari, A. (2015) Caspases in plants: metacaspase gene family in plant stress responses. *Funct. Integr. Genomics,* **15,** 639-649.

Frazão, C., Enguita, F. J., Coelho, R., Sheldrick, G. M., Navarro, J. A., Hervás, M., De la Rosa, M. A., and Carrondo, M. A. (2001). Crystal structure of low-potential cytochrome c549 from *Synechocystis sp*. PCC 6803 at 1.21 Å resolution. *J. Biol. Inorg. Chem.*, **6**, 324–332.

Fujii, Y., Kodama, Y. (2015) In planta comparative analysis of improved green fluorescent proteins with reference to fluorescence intensity and bimolecular fluorescence complementation ability. *Plant Biotech.* **32**, 81-87.

Gandia, J., Galino, J., Amaral, O.B., Soriano, A., Lluís, C., Franco, R. and Ciruela, F. (2008) Detection of higher-order G protein-coupled receptor oligomers by a combined BRET–BiFC technique. *FEBS Lett.* **582**, 2979-2984.

García-Heredia, J.M., Hervás, M., De la Rosa, M.A. and Navarro, J.A. (2008) Acetylsalicylic acid induces programmed cell death in *Arabidopsis* cell cultures. *Planta*, **228**, 89-97.

García-Heredia, J. M., Díaz-Quintana, A., Salzano, M., Orzáez, M., Pérez-Payá, E., Teixeira, M., De La Rosa, M. A., and Díaz-Moreno, I. (2011). Tyrosine phosphorylation turns alkaline transition into a biologically relevant process and makes human cytochrome *c* behave as an anti-apoptotic switch. *J. Biol. Inorg. Chem.*, **16**, 1155–1168.

Giannattasio, S., Atlante, A., Antonacci, L., Guaragnella, N., Lattanzio, P., Passarella, S. and Marra, E. (2008) Cytochrome *c* is released from coupled mitochondria of yeast en route to acetic acid-induced programmed cell death and can work as an electron donor and a ROS scavenger. *FEBS Lett.* **582**, 1519-1525.

González-Arzola, K., Díaz-Moreno, I., Cano-González, A., Díaz-Quintana, A., Velázquez-Campoy, A., Moreno-Beltrán, B., López-Rivas, A. and De la Rosa, M.A. (2015) Structural basis for inhibition of the histone chaperone activity of SET/TAF-Iβ by cytochrome *c*. *Proc. Natl. Acad. Sci. USA,* **112**, 9908-9913.

González-Arzola, K., Díaz-Quintana, A., Rivero-Rodríguez, F., Velázquez-Campoy, A., De la Rosa, M.A., and Díaz-Moreno, I. (2017) Histone chaperone activity of *Arabidopsis thaliana* NRP1 is blocked by cytochrome *c*. *Nucleic Acids Res.* **45**, 2150-2165.

Goñi, G., Herguedas, B., Hervás, M., Peregrina, J. R., De la Rosa, M. A., Gómez-Moreno, C., Navarro, J. A., Hermoso, J. A., Martínez-Júlvez, M., and Medina, M. (2009). Flavodoxin: A compromise between efficiency and versatility in the electron transfer from Photosystem I to Ferredoxin-NADP+ reductase. *Biochim. Biophys. Acta - Bioener*, **1787**, 144–154.

Guerra-Castellano, A., Díaz-Quintana, A., Moreno-Beltrán, B., López-Prados, J., Nieto, P. M., Meister, W., Staffa, J., Teixeira, M., Hildebrandt, P.,

De la Rosa, M. A., and Díaz-Moreno, I. (2015) Mimicking Tyrosine Phosphorylation in Human Cytochrome *c* by the Evolved tRNA Synthetase Technique. *Chem. Eur. J.*, **21**, 15004–15012.

Guerra-Castellano, A., Díaz-Moreno, I., Velázquez-Campoy, A., De La Rosa, M. A., and Díaz-Quintana, A. (2016) Structural and functional characterization of phosphomimetic mutants of cytochrome *c* at threonine 28 and serine 47. *Biochim. Biophys. Acta - Bioener*, *1857*, 387–395.

Guerra-Castellano, A., Díaz-Quintana, A., Pérez-Mejías, G., Elena-Real, C. A., González-Arzola, K., García-Mauriño, S. M., De la Rosa, M. A., and Díaz-Moreno, I. (2018). Oxidative stress is tightly regulated by cytochrome *c* phosphorylation and respirasome factors in mitochondria. *Proc. Natl. Acad. Sci. USA*, *115*, 7955–7960.

Hatsugai, N., Kuroyanagi, M., Yamada, K., Meshi, T., Tsuda, S., Kondo, M., Nishimura, M. and Hara-Nishimura, I. (2004) A plant vacuolar protease, VPE, mediates virus-induced hypersensitive cell death. *Science*, **305**, 855-858.

Hervás, M., Bashir, Q., Leferink, N.G., Ferreira, P., Moreno-Beltrán, B., Westphal, A.H., Díaz-Moreno, I., Medina, M., de la Rosa, M.A., Ubbink, M., Navarro, J.A. and van Berkel, W.J. (2013) Communication between (L)-galactono-1,4-lactone dehydrogenase and cytochrome *c*. *FEBS J.* **280**, 1830-40.

Jaspert, N., Throm, C. and Oecking, C. (2011) *Arabidopsis* 14-3-3 proteins: fascinating and less fascinating aspects. *Front. Plant Sci.* **2**, 96.

Kalpage, H. A., Wan, J., Morse, P. T., Zurek, M. P., Turner, A. A., Khobeir, A., Yazdi, N., Hakim, L., Liu, J., Vaishnav, A., Sanderson, T. H., Recanati, M. A., Grossman, L. I., Lee, I., Edwards, B. F. P., and Hüttemann, M. (2020).

Cytochrome *c* phosphorylation: Control of mitochondrial electron transport chain flux and apoptosis. *Int. J. Biochem. Cell Biol.*, **121**, 105704.

Kim, J., Parrish, A.B., Kurokawa, M., Matsuura, K., Freel, C.D., Andersen, J.L., Johnson, C.E. and Kornbluth, S. (2012) Rsk-mediated phosphorylation and 14-3-3ε binding of Apaf-1 suppresses cytochrome *c*-induced apoptosis. *EMBO J.* **31**, 1279-1292.

Kimura, M. The neutral theory of molecular evolution, *Cambridge University Press*, Cambridge, UK, 1983.

Lalle, M., Visconti, S., Marra, M., Camoni, L., Velasco, R. and Aducci, P. (2005) ZmMPK6, a novel maize MAP kinase that interacts with 14-3-3 proteins. *Plant Mol. Biol.* **59**, 713-722.

Li, P., Nijhawan, D., Budihardjo, I., Srinivasula, S.M., Ahmad, M., Alnemri, E.S. and Wang, X. (1997) Cytochrome *c* and dATP-dependent formation of Apaf-1/caspase-9 complex initiates an apoptotic protease cascade. *Cell,* **91**, 479-489.

Martínez-Fábregas, J., Díaz-Moreno, I., González-Arzola, K., Janocha, S., Navarro, J.A., Hervás, M., Bernhardt, R., Díaz-Quintana, A. and De la Rosa M.Á. (2013) New *Arabidopsis thaliana* cytochrome *c* partners: a look into the elusive role of cytochrome *c* in programmed cell death in plants. *Mol. Cell. Proteomics*, **12**, 3666-3676.

Martínez-Fábregas, J., Díaz-Moreno, I., González-Arzola, K., Janocha, S., Navarro, J.A., Hervás, M., Bernhardt, R., Velázquez-Campoy, A., Díaz-Quintana, A. and De la Rosa, M.A. (2014a) Structural and functional analysis of novel human cytochrome *c* targets in apoptosis. *Mol. Cell. Proteomics,* **13**, 1439-1456.

Martínez-Fábregas, J., Díaz-Moreno, I., González-Arzola, K., Díaz-Quintana, A. and De la Rosa, M.A. (2014b) A common signalosome for programmed cell death in humans and plants. *Cell Death Dis.* **5**, e1314.

Masters, S.C., Pederson, K.J., Zhang, L., Barbieri, J.T. and Fu, H. (1999) Interaction of 14-3-3 with a nonphosphorylated protein ligand, exoenzyme S of *Pseudomonas aeruginosa*. *Biochemistry*, **38**, 5216-5221.

rvás, M., Navarro, J. A., De la Rosa, M. A., Gómez-Moreno, C., and Tollin, G. (1992). A laser flash absorption spectroscopy study of *Anabaena* sp. PCC 7119 flavodoxin photoreduction by photosystem I particles from spinach. *FEBS Lett.*, **313**, 239–242.

Moreno-Beltrán, B., Díaz-Quintana, A., González-Arzola, K., Velázquez-Campoy, A., De la Rosa, M.A. and Díaz-Moreno, I. (2014) Cytochrome c_1 exhibits two binding sites for cytochrome *c* in plants. *Biochim. Biophys. Acta Bioenerg.* **1837**, 1717-1729.

Moreno-Beltrán, B., Díaz-Moreno, I., González-Arzola, K., Guerra-Castellano, A., Velázquez-Campoy, A., De la Rosa, M.A. and Díaz-Quintana, A. (2015) Respiratory complexes III and IV can each bind two molecules of cytochrome *c* at low ionic strength. *FEBS Lett.* **589**, 476-483.

Moreno-Beltrán, B., Guerra-Castellano, A., Díaz-Quintana, A., Del Conte, R., García-Mauriño, S.M., Díaz-Moreno, S., González-Arzola, K., Santos-Ocaña, C., Velázquez-Campoy, A., De la Rosa, M.A., Turano, P. and Díaz-Moreno, I. (2017) Structural basis of mitochondrial dysfunction in response to cytochrome *c* phosphorylation at tyrosine 48. *Proc. Natl. Acad. Sci. USA,* **114**, E3041-E3050.

Muslin, A.J., Tanner, J.W., Allen, P.M. and Shaw, A.S. (1996) Interaction of 14-3-3 with signaling proteins is mediated by the recognition of phosphoserine. *Cell*, **84**, 889-897.

Nagaoka, N., Yamashita, A., Kurisu, R., Watari, Y., Ishizuna, F., Tsutsumi, N., Ishizaki, K. and Kohchi, T. (2017) DRP3 and ELM1 are required for mitochondrial fission in the liverwort *Marchantia polymorpha*. *Sci. Rep.* **7**, 4600.

Navarro, J. A., Hervas, M., De la Cerda, B., and De la Rosa, M. A. (1995a). Purification and physicochemical properties of the low potential cytochrome c549 from the cyanobacterium *Synechocystis sp* PCC 6803. *Arch. Biochem. Biophys.*, **318**, 46–52.

Navarro, J. A., Hervás, M., Genzor, C. G., Cheddar, G., Fillat, M. F., de la Rosa, M. A., Gómez-Moreno, C., Cheng, H., Xia, B., Chae, Y. K., Yan, H., Wong, B., Straus, N. A., Markley, J. L., Hurley, J. K., and Tollin, G. (1995b). Site-specific mutagenesis demonstrates that the structural requirements for efficient electron transfer in Anabaena ferredoxin and flavodoxin are highly dependent on the reaction partner: Kinetic studies with photosystem I, Ferredoxin:NADP+ Reductase. *Arch. Biochem. Biophys.*, **321**, 229–238.

Nelson, B.K., Cai, X. and Nebenführ, A. (2007) A multicolored set of *in vivo* organelle markers for co-localization studies in *Arabidopsis* and other plants. *Plant J.,* **51**, 1126-1136.

Nomura, M., Shimizu, S., Sugiyama, T., Narita, M., Ito, T., Matsuda, H. and Tsujimoto, Y. (2002) 14-3-3 interacts directly with and negatively regulates pro-apoptotic Bax. *J. Biol. Chem.* **278**, 2058-2065.

Petosa, C., Masters, S.C., Bankston, L.A., Pohl, J., Wang, B., Fu, H. and Liddington, R.C. (1998) 14-3-3ζ binds a phosphorylated Raf peptide and an unphosphorylated peptide via its conserved amphipathic groove. *J. Biol. Chem.* **273**, 16305-16310.

Pettersen, E.F., Goddard, T.D., Huang, C.C., Couch, G.S., Greenblatt, D.M., Meng, E.C. and Ferrin, T.E. (2004) UCSF Chimera – A visualization system for exploratory research and analysis. *J. Biol. Chem.* **25**, 1605-1612.

Piotto, M., Saudek, V. and Sklenár, V. (1992) Gradient-tailored excitation for single-quantum NMR spectroscopy of aqueous solutions. *J. Biomol. NMR,* **2**, 661-665.

Riedl, S.J., Li, W., Chao, Y., Schwarzenbacher, R. and Shi, Y. (2005) Structure of the apoptotic protease-activating factor 1 bound to ADP. *Nature*, **434**, 926-933.

Rodríguez-Roldán, V., García-Heredia, J.M., Navarro, J.A., Hervás, M., De la Cerda, B., Molina-Heredia, F.P. and De la Rosa, M.A. (2006) A comparative kinetic analysis of the reactivity of plant, horse, and human respiratory cytochrome *c* towards cytochrome *c* oxidase. *Biochem. Biophys. Res. Commun.* **346**, 1108-1113.

Rodríguez-Roldán, V., García-Heredia, J.M., Navarro, J. A., De la Rosa, M. A., and Hervás, M. (2008) Effect of nitration on the physicochemical and kinetic features of wild-type and monotyrosine mutants of human respiratory cytochrome *c*. *Biochemistry*. **47,** 12371-12379.

Rueden, C.T., Schindelin, J., Hiner, M.C., DeZonia, B.E., Walter A.E., Arena E.T., and Eliceiri, K.W. (2017) ImageJ2: ImageJ for the next generation of scientific image data. *BMC Bioinform*. 18, 529-555.

Sievers, F., Wilm, A., Dineen, D., Gibson, T.J., Karplus, K., Li, W., Lopez, R., McWilliam, H., Remmert, M., Söding, J., Thompson, J.D. and Higgins, D.G. (2011) Fast, scalable generation of high-quality protein multiple sequence alignments using Clustal Omega. *Mol. Syst. Biol.* **7**, 539.

Sun, J., Xu, W., Hervás, M., Navarro, J. A., De La Rosa, M. A., and Chitnis, P. R. (1999. Oxidizing side of the cyanobacterial photosystem I. Evidence for interaction between the electron donor proteins and a luminal surface helix of the PsaB subunit. *J. Biol. Chem.*, **274**, 19048–19054.

Uversky, V.N., Pallucca, R., Visconti, S., Camoni, L., Cesareni, G., Melino, S., Panni, S., Torreri, P. and Aducci, P. (2014) Specificity of ε and non-ε isoforms of *Arabidopsis* 14-3-3 proteins towards the H^+-ATPase and other targets. *PLoS ONE,* **9**, e90764.

van Kleeff, P.J.M., Jaspert, N., Li, K.W., Rauch, S., Oecking, C. and de Boer, A.H. (2014) Higher order Arabidopsis 14-3-3 mutants show 14-3-3 involvement in primary root growth both under control and abiotic stress conditions. *J. Exp. Bot.* **65**, 5877-5888.

Walter, M., Chaban, C., Schütze, K., Batistic, O., Weckermann, K., Näke, C., Blazevic, D., Grefen, C., Schumacher, K., Oecking, C., Harter, K. and Kudla, J. (2004) Visualization of protein interactions in living plant cells using bimolecular fluorescence complementation. *Plant J.* **40**, 428-438.

Yan, J., He, C., Wang, J., Mao, Z., Holaday, S.A., Allen, R.D. and Zhang, H. (2004) Overexpression of the Arabidopsis 14-3-3 protein GF14λ in cotton leads to a “stay-green” phenotype and improves stress tolerance under moderate drought conditions. *Plant Cell Physiol.* **45,** 1007-1014.

Yang, X., Lee, W.H., Sobott, F., Papagrigoriou, E., Robinson, C.V., Grossmann, J.G., Sundström, M., Doyle, D.A. and Elkins, J.M. (2006) Structural basis for protein-protein interactions in the 14-3-3 protein family. *Proc. Natl. Acad. Sci. USA,* **103**, 17237-42.

Yoo, S.D., Cho, Y.H. and Sheen, J. (2007) *Arabidopsis* mesophyll protoplasts: a versatile cell system for transient gene expression analysis. *Nat. Protoc*. **2**,1565-1572.

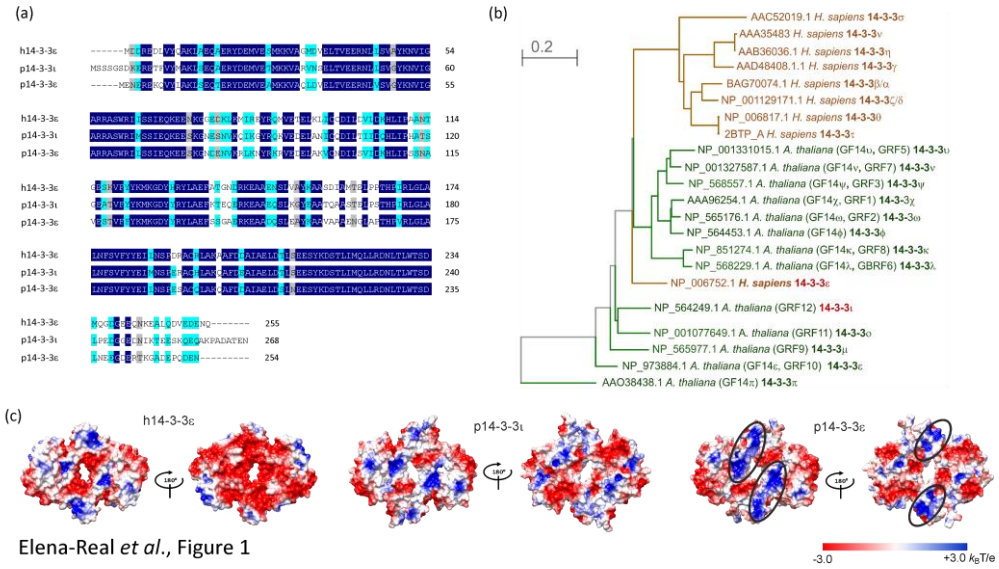

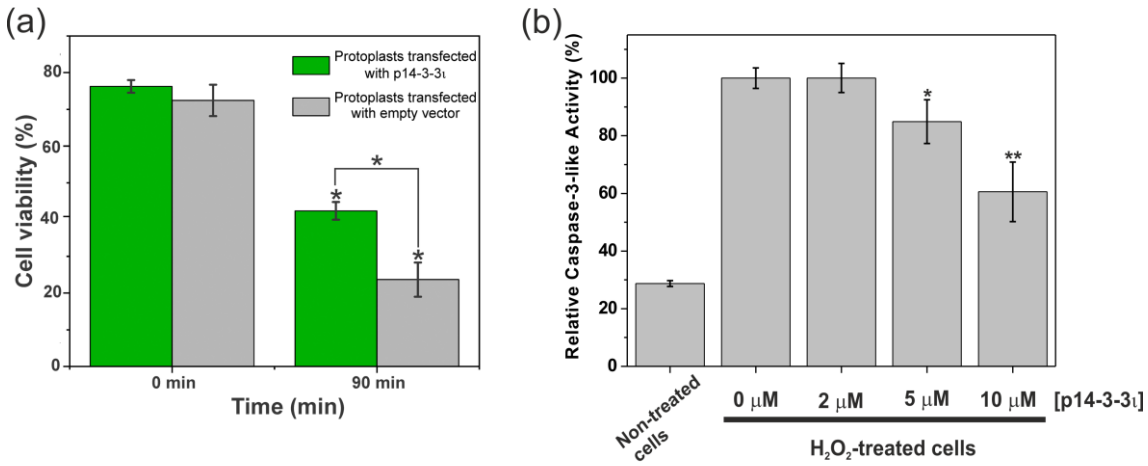

Elena-Real *et al.*, Figure 2

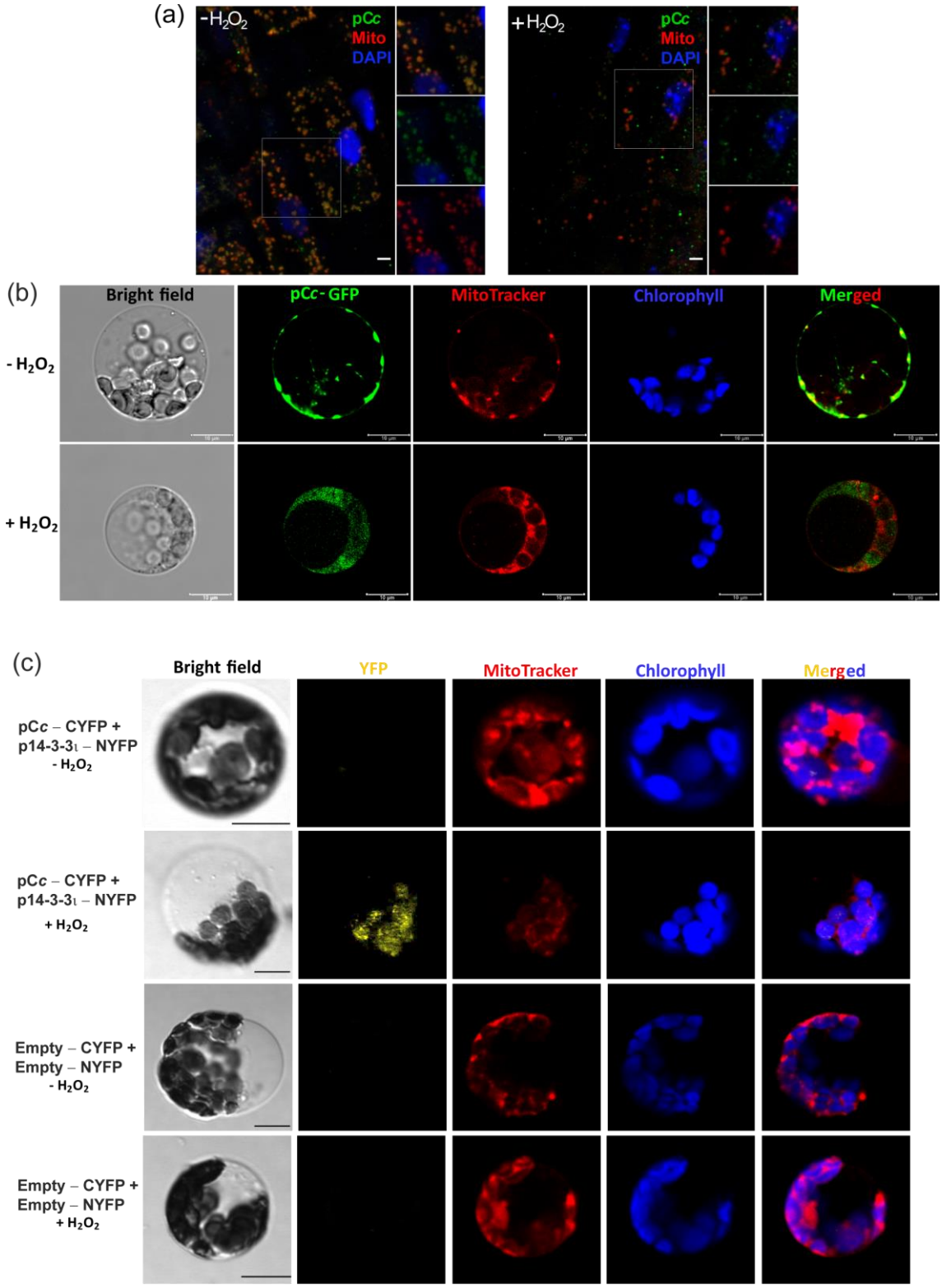

Elena-Real *et al.*, Figure 3

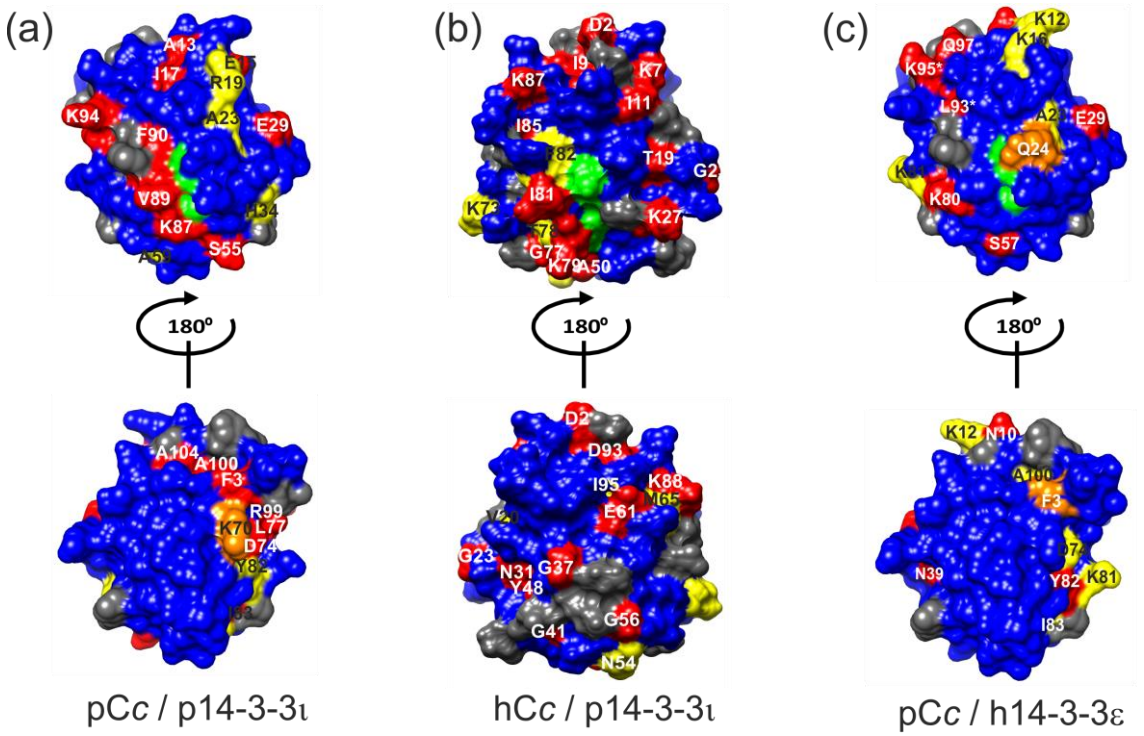

K_D = 8.5 μM ΔH = 1.4 kcal mol^{-1} n = 1.9	K_D = 2.8 μM ΔH = 2.9 kcal mol^{-1} n = 1.6	K_D = 29 μM ΔH = 1.9 kcal mol^{-1} n = 1.6

Elena-Real *et al.*, Figure 4

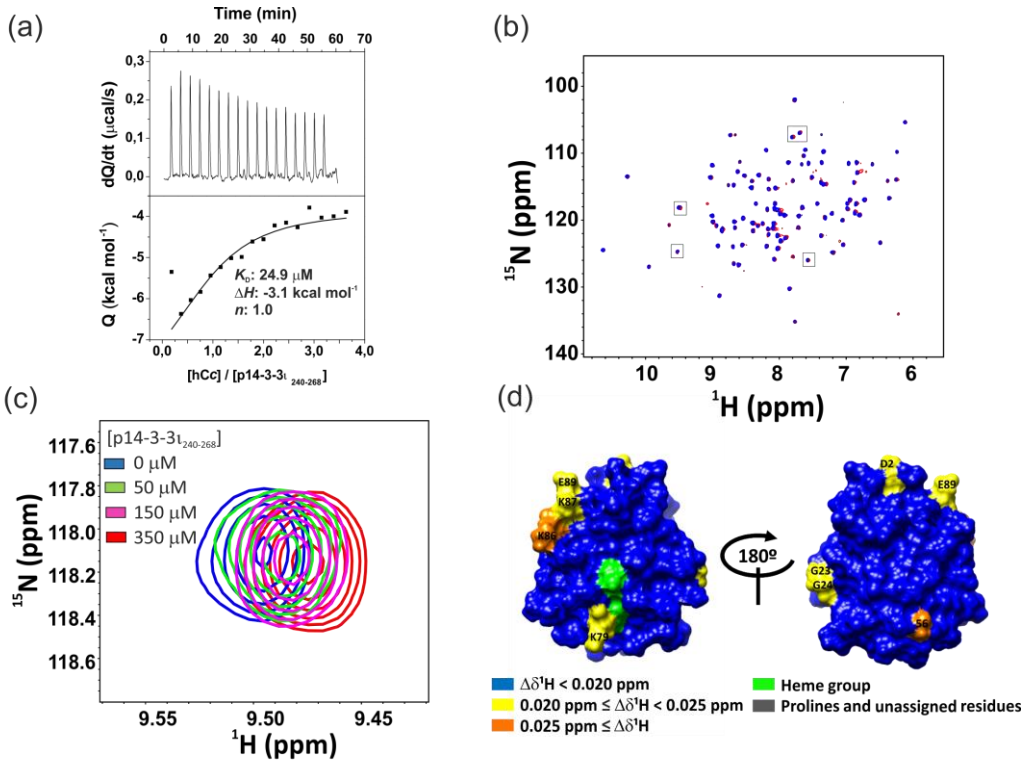

Elena-Real *et al.*, Figure 5

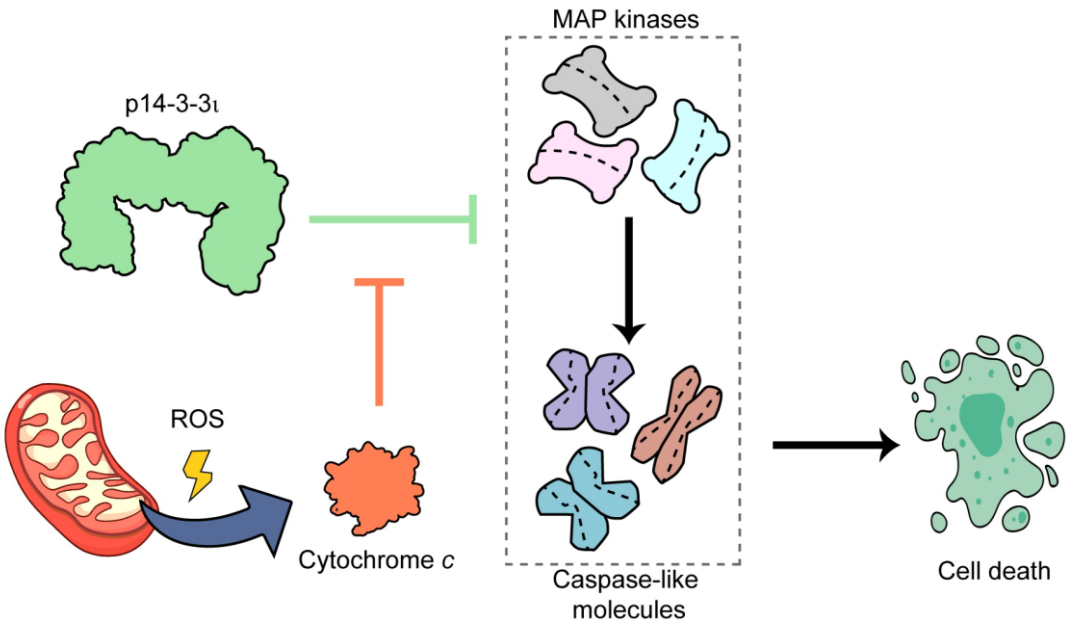

FIGURE LEGENDS

Figure 1. Comparison between plant and human 14-3-3 family member isoforms

(a) Multiple alignment of human 14-3-3ε (h14-3-3ε; UniProt entry: P62258), plant 14-3-3ι (p14-3-3ι; Q9C5W6) and plant 14-3-3ε (p14-3-3ε; P48347) amino-acid sequences, using the Clustal Omega program (Sievers *et al*., 2011). Sequences are colored by similarity: fully conserved residues in dark blue, residues with strongly similar properties in light blue and residues with weakly similar properties in gray. **(b)** Evolutionary relationship between *H. sapiens* 14-3-3ε and its orthologous *A. thaliana* isoforms. Cladogram obtained from sequence alignments of the distinct thirteen plant 14-3-3 isoforms using BLASTp 2.9.0 (Altschul *et al.*, 1997) by the Fast Minimum Evolution algorithm (Desper & Gascuel, 2004). Evolutionary distances correspond to the expected fraction of amino acid substitutions per site according to the fraction of mismatches in the alignment (Kimura, 1983). The members of the *A. thaliana* 14-3-3-like group are in green, whereas the human 14-3-3 isoforms are in brown. **(c)** Electrostatic surface potential of h14-3-3ε, p14-3-3ι and p14-3-3ε proteins (residues 1-233, 1-239 and 1-234, respectively). Negatively and positively charged regions of the three protein surfaces are depicted in red and blue, respectively. The color scale ranges from -3 (red) to +3 (blue) *k*BT. Black circles stand for positively-charged regions prominent in p14-3-3ε. The simulation was performed using APBS (Baker *et al*., 2001) aided by Chimera (Pettersen *et al*., 2004), assuming an ionic strength of 100 mM.

Figure 2. Effect of p14-3-3ι on cell viability and caspase-3-like activity of *A. thaliana* cells.

(a) Viability of *A. thaliana* MM2d protoplasts transfected with p14-3-3ι or empty vectors upon oxidative stress. Both type of protoplasts was treated with 35 mM H_2O_2. Viability was followed by dyeing viable cells with fluorescein diacetate (FDA). **(b)** Relative caspase-3-like activity in non-treated and H_2O_2-treated MM2d cell extracts were measured after 18 h incubation with the fluorescent substrate for human caspase-3 (Ac-DEVD-AMC). p14-3-3ι at varying concentration was

added to H_2O_2-treated cell extracts, as indicated. Data shows the mean value ±SD of three independent experiments. Asterisks indicate statistically significant differences (*p < 0.05; **p < 0.01).

Figure 3. Release of plant C*c* into the cytosol in MMd2 cells upon oxidative stress and its binding to plant 14-3-3ι.

(a) pC*c* release from mitocondria upon oxidative stress in 35S:Mt-YFP *Arabidopsis* roots. Four-day-old plants expressing YFP in the mitocondria (35S:Mt-YFP) were mock-treated (*left*) or treated with 35 mM H_2O_2 for 4h (*right*). Immunolocalization was performed to detect pC*c* (green) and YFP (red). Nuclei were stained with DAPI (blue). Scale bar: 2 µm. **(b)** *A. thaliana* protoplasts were transfected with the p35S-pC*c*-sfGFP vector to corroborate *in vivo* localization of GFP fusion protein in the presence or absence of 35 mM H_2O_2 for 4 h. GFP fluorescence (green), chlorophyll autofluorescence (blue) and mitochondria stained with MitoTracker Red CMX-Ros (red) were examined by confocal laser-scanning microscopy. Scale bar: 10 µm. **(c)** *A. thaliana* protoplasts were transfected with pSPYCE/pSPYNE vectors to corroborate *in vivo* interaction of pC*c* with p14-3-3ι by BiFC. Images were captured 24 h after transient transfection and 90 min after treatment with 35 mM H_2O_2. Reconstruction of YFP leads to green fluorescence emission, indicative of interaction between pC*c* and its protein partner. Scale bar: 10 µm. See details in Materials and Methods.

Figure 4. Binding of plant C*c* and 14-3-3ι proteins, as compared with the heterologous complexes.

Mappings of plant C*c* surface residues perturbed at the complex with plant 14-3-3ι protein **(a)**, and those of the heme protein at the cross complexes **(b, c)**. The C*c*:14-3-3 ratio is 1:0.75 in the three complexes. Residues are colored according to their ^1H $\Delta\Delta\nu_{1/2Binding.}$ Resonances broaden beyond the threshold corresponding to the average plus 1-fold standard deviation (16.38 Hz in a, 36.99 Hz in b and 38.20 Hz in c) are in yellow. Signals with a line-width larger than the average plus

2-fold standard deviation (23.28 Hz in a, 50.76 Hz in b and 50.38 Hz in c) are in red. Residues with average chemical-shift perturbations ($\Delta\delta_{avg}$) larger than 0.035 ppm are represented in orange. Residues without substantial ^{1}H $\Delta\Delta\nu_{1/2Binding}$ and $\Delta\delta_{avg}$ are in blue. Prolines and non-assigned residues are in gray. The heme group is in green. The equilibrium dissociation constant (K_D), enthalpy change (ΔH) and stoichiometry (n) of the three interactions are in the square below.

Figure 5. Binding assays of hC*c* / p14-3-3ι$_{240-268}$ complex.

(a) ITC binding assay for hC*c* / p14-3-3ι$_{240-268}$. Thermogram and binding isotherm (*top* and *bottom*, respectively) are shown. **(b)** Superimposed ^{15}N-HSQC spectra of ^{15}N-labeled hC*c*, which is either free (blue) or bound to 14-3-3ι$_{240-268}$ at a hC*c*:p14-3-3ι$_{240-268}$ molar ratio of 1:7. **(c)** Details of superimposed ^{15}N-HSQC spectra of ^{15}N-labeled hC*c* upon titration with p14-3-3ι$_{240-268}$. The C*c* concentration was 50 μM at each titration step. Signals corresponding to distinct titration steps are colored according to the code in the panel. The p14-3-3ι$_{240-268}$ concentration at each titration step is depicted in the legend. **(d)** CSP map of hC*c* upon addition of p14-3-3ι$_{240-268}$. hC*c* surfaces are rotated 180° around vertical axes in each view. Residues are colored according to their respective average chemical-shift perturbations value, as the panel shows.

Figure 6. Proposed model of plant programmed cell death modulation by cytochrome *c*-dependent p14-3-3ι inhibition. ROS production in response to H_2O_2-treatment makes plant C*c* release from mitochondria and inhibit p14-3-3ι in the cytoplasm. In this way, C*c* contributes to programmed cell death by preventing p14-3-3ι from blocking caspase-like molecules.